Effect of thin polymer film's confinement on the Formation of Laser-Induced Periodic Surface Structures on Silicon

Mengyuan Wang[1], Shengying Lai[1*], Haijun Zhao[1], Siyi Zhang[1], Chunchun Fei[1] , and Bing Han[2]

[1]*School of Mathematics, Physics and Statistics, Shanghai University of Engineering Science, Longteng Road 333, Shanghai 201620, China*
[2]*School of Electronic and Optical Engineering, Nanjing University of Science and Technology, Nanjing 210094, China*
**Corresponding author's e-mail: shengyinglai@sues.edu.cn*

Laser-based patterning of high-quality submicron patterns on large-area substrates remains a significant challenge. In this study, photoresist films of varying thicknesses are deposited on silicon surfaces by spin coating to achieve patterning. The samples are exposed to nanosecond laser pulses (λ = 532 nm, τ = 8 ns). The formation of laser-induced periodic surface structures (LIPSS) on silicon surface when restricted by the photoresist film in air was investigated. The results show that the period of LIPSS on the silicon surface remains consistent (~530 ± 5 nm) under different film thickness (d = 420 nm and 620 nm). With the constraint of photoresist film, the minimum threshold for LIPSS formation on the silicon surface was ~14 mJ/cm² (d = 420 nm). The formation mechanism of LIPSS is attributed to the interference between the incident laser beam and surface scattering waves, as well as plasma enhancement within the confined layer. Studies have shown that by restricting plasma within the thin film to prepare wavelength periodic structures on the silicon surface, the energy coupling efficiency in laser direct writing can be significantly enhanced, thereby improving the laser-material interaction effect. This study provides important references and support for the potential applications of laser micro processing technology in layered structures.

DOI: 10.2961/jlmn.2026.02.2001
Keywords: laser processing, laser-induced periodic surface structures (LIPSS), thin film thickness, plasma enhancement

1. Introduction

Laser-matter interactions, particularly on material surfaces, have garnered significant research attention in recent years due to their capacity to generate diverse micro- and nanostructures. Among them, laser-induced periodic surface structures (LIPSS) are particularly noteworthy [1-4]. This structure is characterized by regular wavelength ripples that frequently appear on the surfaces of various materials when exposed to laser irradiation. As a quintessential semiconductor material, silicon finds ubiquitous applications in several rapidly advancing technological fields, such as silicon photonics, solar cells, and integrated circuits [5, 6].Consequently, the fabrication of high-quality and controllable LIPSS on silicon surfaces represents a technologically crucial objective. However, the direct generation of homogeneous and high-fidelity LIPSS on elemental silicon is significantly challenged by its inherent material properties: a high absorption coefficient leading to intense localized heating, high thermal conductivity promoting rapid heat dissipation inhibiting localized phase changes required for LIPSS formation [7]. To address these limitations, the novel approach of thin-film confinement has emerged. This strategy involves coating the substrate surface with a thin film layer designed to modulate the laser-matter interaction. This modulation effectively reduces thermal damage to the underlying silicon substrate while simultaneously facilitating the formation of LIPSS on the target surface.

Existing thin film confinement studies have primarily focused on metal (Au [8], Ag [9], Al [10], etc.) or dielectric (SiO_2) thin films. Metal thin film research has mainly focused on exciting surface plasmon polaritons (SPPs) [11], while dielectric thin film research has focused on optical properties and their role as confinement layers. Unlike metals and media, the mechanisms by which polymer materials interact with lasers are extremely diverse. The formation of micro- and nanostructures in polymers involves the rearrangement of polymer chains, amorphisation of crystalline domains, local surface melting, ablation, photolytic shrinkage, and photo oxidation, that occur during this process. And the transport and rearrangement of materials further affects the formation of ripples, which ultimately leads to the generation of multiple characteristic surface structures. It is worth noting that the vaporization process of materials under pulsed laser irradiation produces plasma plumes.

Irradiation of the material surface by a pulsed laser generates plasma [12], which is an important intermediate step in the formation process of LIPSS. The main characteristics of plasma are high temperature, high pressure and high density, and its formation process is accompanied by strong shock waves. The deposition of laser energy on the material surface triggers localized ionization, leading to the rapid evaporation of the surface material and the formation of a plasma cloud. The properties and behavior of the plasma are influenced by the laser conditions (e.g. pulse width, fluence,

and wavelength) as well as by the environmental conditions (e.g. air pressure and gas type). The intensity of the plasma radiation can be analyzed by emission spectroscopy, which is used to study the composition and structure of matter. For example, Matsuta et al. [13] used an Nd laser (190 mJ, 10 ns) to induce a copper plasma. The strongest intensity of plasma radiation was found to be obtained in an Ar gas environment of about 4×10^3 Pa. Compared with conventional nanosecond lasers, ultrashort pulsed lasers are able to excite the plasma through nonlinear interactions at lower pulse energies due to their higher electric field strength. Simultaneously, the plasma contains a high density of free electrons, which can support the generation of surface plasmon polaritons (SPPs) at the plasma-air interface. These SPPs interact with external electromagnetic fields, leading to a significant enhancement of the electromagnetic field intensity in the local region. This localized field enhancement further promotes laser-material interaction, leading to the formation of periodic energy distributions on the material surface and thereby driving the generation of LIPSS. Especially at high electric field strengths, the synergistic effect of plasma and SPP can precisely modulate the morphology and periodicity of surface microstructures [14]. However, in open processing environments, the generated plasma rapidly expands and diffuses, leading to rapid energy dissipation. This reduces the utilization efficiency of laser energy and compromises the controllability of the processing process. To more effectively harness plasma energy and control the dynamic process, confinement techniques are widely adopted. Zimmer et al. [15] attached non-absorbent liquids (water and acetone) to the metal absorber layer. Lai et al [16] investigated the formation mechanisms of laser-induced rippled structures in both aqueous and air environments. Ehrhardt et al. [17] devised a layered system between a thin interlayer placed between the SiO_2 substrate and the metal absorber. In order to investigate the effect of the confinement on the etching characteristics and the generated LIPSS, they deposited thick polymer layers of different thicknesses on the metal absorber as a confining layer for experimental analysis.

This study investigates the formation mechanism of LIPSS on silicon under polymer film confinement using nanosecond pulsed lasers, as there is currently a lack of knowledge regarding the mechanism of laser ablation of silicon under confined conditions. The objective of this study is to achieve micro-nano structures on silicon surfaces by restricting them with polymer films of varying thicknesses. Detailed analyses were conducted on the morphological changes observed after laser irradiation. Laser ablation of silicon under polymer film constraints was performed under different laser fluences and laser pulse numbers. This work holds significant value for investigating the application of LIPSS in laser microfabrication of silicon under polymer film constraints.

2. Experimental techniques and materials

A schematic view of the laser irradiation is shown in **Figure 1**. The set-up comprises the nanosecond laser system, optics for guiding, attenuation and focusing the laser beam, a 3-dimension stage system for sample movement and an energy meter for the measurement of laser pulse energy. The laser used in the experiment is a solid-state laser system (Vlite-200, Beamtech Optronics Co., Ltd.) with a wavelength of λ=532 nm and a pulse width of τ=8 ns. The repetition frequency is continually adjustable from 1 Hz to 15 Hz. The maximum pulse energy is 200 mJ. The laser beam with a flat-top beam profile has a vertical polarization direction after beam shaping. The laser beam is focused on the sample surface with a spot size of 40 ± 5μm. The sample is fixed on the three-dimensional workbench and the movement precision of the workbench can reach to 10 μm.

The experiments are constructed with laser irradiation on a photoresist/silicon substrate system. The substrate wafer is a single-side polished wafer with a thickness of 380 μm.The photoresist is positive resists (AZ ECI 3027). The silicon wafer is cleaned by propanol and deionized water before the experiments. After cleaning, the photoresist is deposited on the surface of the silicon wafer substrate by spin coating method with a speed of 2000 rpm and 2500rpm, respectively. After deposition, the sample is backed at 90℃ for 2 min. The thickness of the photoresist of ~620nm and ~420nm is measured by the white light interferometer.

After laser irradiation, the samples are examined without further cleaning. The surface morphologies are analyzed by optical microscope (OM, DMM-330C, Caikang Optics) and scanning electron microscopy (SEM, SU8010 and S-3400N from Hitachi). Thin platinum film is deposited for SEM imaging by magnetron sputtering.

3. Results

The laser fluences chosen for the experiments ranged from 1043 mJ/cm² to 113 mJ/cm² while the used number of laser pulses was increased from N = 1 to 10. After laser irradiation of photoresists with different film thicknesses, the generated morphologies were analyzed using SEM and OM. We classify them into six categories, as shown in **Table 1**. **Figure 2** illustrates the typical morphology of each category.

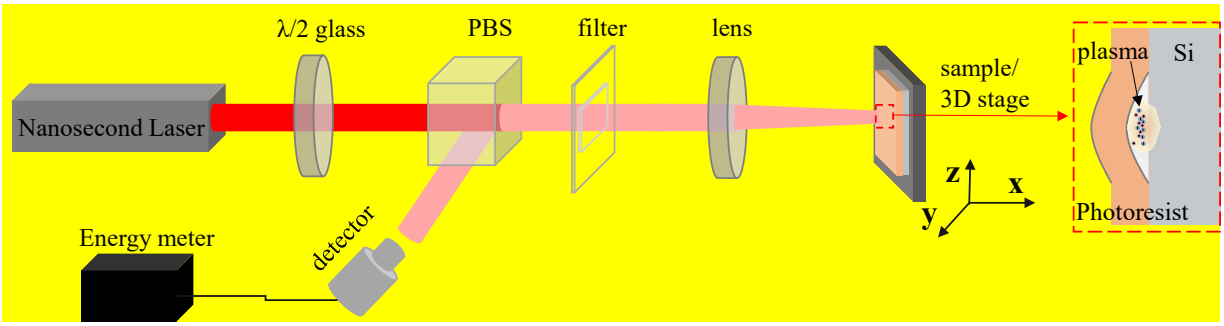

Fig.1 Schematic view of the experimental setup for laser irradiation of the samples.

(A) The dark red area in **Table 1** indicates silicon ablation. The ablation of the silicon samples with photoresist is performed by the silicon at the center of the laser irradiation. The morphology of laser ablation is shown in **Figure 2(a)**.

(B) The red area in **Table 1** indicates that silicon has undergone melting. Laser irradiation resulted in the melting of the silicon surface, which presented a flowing state with small pits. The characteristic morphology is shown in **Figure 2(b).**

(C) The green area in **Table 1** indicates silicon melting accompanied by the formation of LIPSS. The laser-induced LIPSS shows periodic grating-like stripes. The morphology is shown in **Figure 2(h)**.

(D) The yellow area in **Table 1** indicates photoresist melting. The photoresist sticks together and exhibits a curled-up shape. The morphology is shown in **Figure 2(d)**.

(E) The orange area in **Table 1** indicates photoresist rupture. The surface of the photoresist under laser action breaks up into irregular pieces, and a small amount of the splashes outside the laser action point. The morphology is shown in **Figure 2(e)**.

(F) The flesh-coloured area in **Table 1** indicates the surface modification of the photoresist. As shown in **Figure 2(f)**. The surface modification of photoresist is caused by low-density laser irradiation. When observed under a microscope, the chemical reaction (photolysis) occurs on the surface of the film and is manifested as a change in the reflected colour of the surface. However, the surface morphology is not altered by SEM imaging.

Figure 3 shows SEM images of the variation of 620 nm photoresist surface morphologies with decreasing laser fluences at a fixed pulse number of 5. At high laser fluence, the temperature of the silicon substrate is above the melting point and the surface of silicon shows ablation phenomenon, as shown in **Figure 3(f)**. As the laser fluence decreases, melting occurs on the surface morphology of the silicon substrate near its melting point, as shown in **Figure 3(e)**.At lower laser fluences, only the disappearance of photoresist on the surface of the silicon substrate is revealed, as shown **in Figure 3(c)**. The melted photoresist manifests itself at low laser fluences, as shown **in Figure 3(b)**. At even lower fluences, the surface ruptures due to mechanical factors, as shown by the photoresist fragments formed **in Figure 3(a)**. At the same time, some irregular features such as splashes,craters and pores were observed on the silicon surface. The LIPSS structure forms within a specific energy range, as shown in **Figure 3(d)**. Specifically, when the photoresist is completely removed and the silicon substrate undergoes only slight surface melting.

Table 1 Changes in surface morphology at different laser energy densities under spin-coating (a) 420 nm photoresist and (b) 620 nm photoresist on silicon samples.

(a) 420nm photoresist on silicon

Laser pulse number *N*	Fluence *F* (mJ/cm²)																																						
	1043	893	821	791	735	643	608	543	513	499	439	413	392	366	341	322	319	301	266	252	240	237	227	224	214	209	206	198	180	163	155	151	145	139	134	127	124	118	115	113
1	Ablation of Si							Melting of Si				LIPSS formation																		Surface modification											
3																																				Cracking of PR				
5																										Melting of PR													
10																																								

(b) 620nm photoresist on silicon

Laser pulse number *N*	Fluence *F* (mJ/cm²)																																						
	1043	893	821	791	735	643	608	543	513	499	439	413	392	366	341	322	319	301	266	252	240	237	227	224	214	209	206	198	180	163	155	151	145	139	134	127	124	118	115	113
1	Ablation of Si							Melting of Si				LIPSS formation										Melting of PR								Cracking of PR										
3																																						Surface modification		
5																																								
10																																								

Ablation of Si | Melting of Si | LIPSS formation | Melting of PR

Cracking of PR | Surface modification | no modification

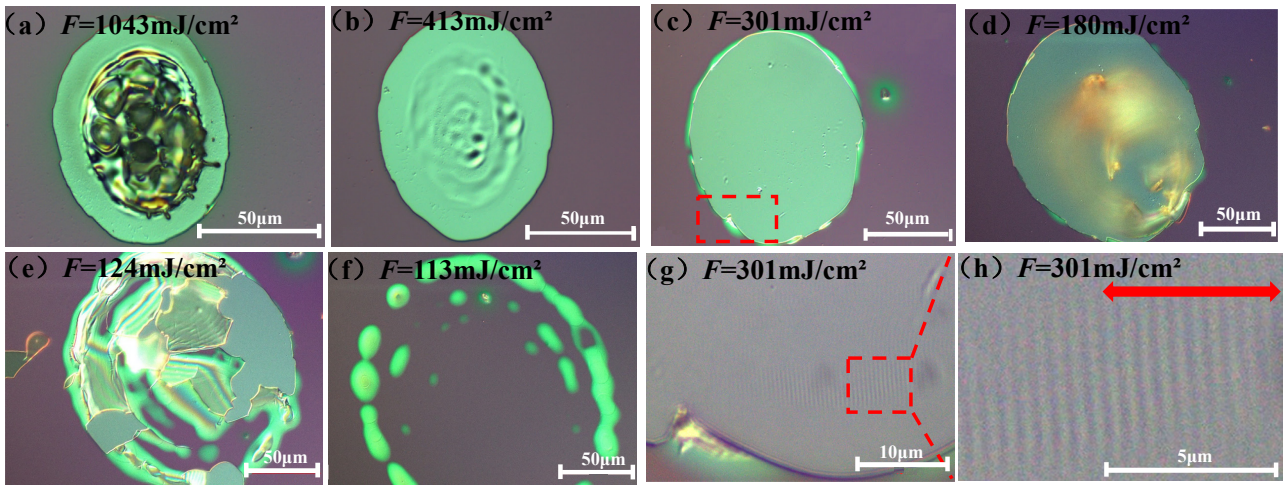

Fig. 2 OM images of the surface topography of 620 nm photoresist irradiated with different laser fluences, (a) F=1043 mJ/cm², (b) F=413 mJ/cm², (c) F=301 mJ/cm², (d) F=180 mJ/cm², (e) F=124 mJ/cm² and (f) F=113 mJ/cm². Fig. 2(g) is an enlarged view of the red dashed box in Fig. 2(c) and Fig. 2(h) is an enlarged view of the red dashed box in Fig. 2(g). The red arrow indicates the direction of polarization of the laser beam. The number of laser pulses is N=10.

Figure 4 shows the minimum threshold variation of each morphology for 420 nm and 620 nm photoresist film thickness at different number of laser pulses (N=1, 3, 5, 10). **Figure 4(a)** represents the trend of morphology thresholds for 420 nm photoresist film thickness with the increase of the number of laser pulses. As the number of laser pulses increases, there was an overall decreasing trend in the minimum threshold for each morphology. This is consistent with the fact that the larger laser pulse number has a greater effect on the laser-actuated surface. Among them, the topographic threshold of silicon ablation decreases the most. The lowest threshold for silicon ablation is 821 mJ/cm² for laser pulse number N=1, and the lowest threshold for silicon ablation is 499 mJ/cm² for pulse number increasing to N=10. The threshold for silicon melting increases slightly for laser pulse number of N=3, which is more evident in **Figure 4(b)**. The thresholds for rupture and melting of the photoresist as well as for the generation of LIPSS and silicon melting do not differ much for pulse numbers 5 and 10.

Figure 4(b) represents the trend of morphology threshold for 620 nm photoresist film thickness with increasing laser pulse number. The silicon melting as well as silicon ablation thresholds are slightly increased for laser pulse number N=5. The other trends are similar to **Figure 4(a)**. The presence of LIPSS was not observed for both 420 nm and 620 nm photoresist film thickness at laser pulse number N=1. Additionally, under constant pulse number conditions, the minimum thresholds for each morphology exhibit a slight downward trend as the membrane layer thickness increases.When the pulse number N = 10, the silicon ablation threshold for a 420 nm thin film thickness was 499 mJ/cm², and the silicon ablation threshold for a 620 nm thin film thickness was 439 mJ/cm².

4. Discussion

The formation of LIPSS was observed when the photoresist/silicon substrate was irradiated using a pulsed laser at a wavelength of 532 nm. The photoresist/silicon substrate surface exhibits different morphological changes when the laser fluence is reduced. These changes were clearly observed under OM and SEM.

Under high laser fluence conditions, when the laser fluence exceeds the ablation threshold of silicon (F=439 mJ/cm², d=620 nm, N=10), the surface temperature of the silicon substrate rapidly rises above its melting temperature (~1687 K), resulting in significant ablation (**Figure 2(a)** and **Figure 3(f)**). This ablation is primarily attributed to a local temperature increase induced by the photothermal effect and

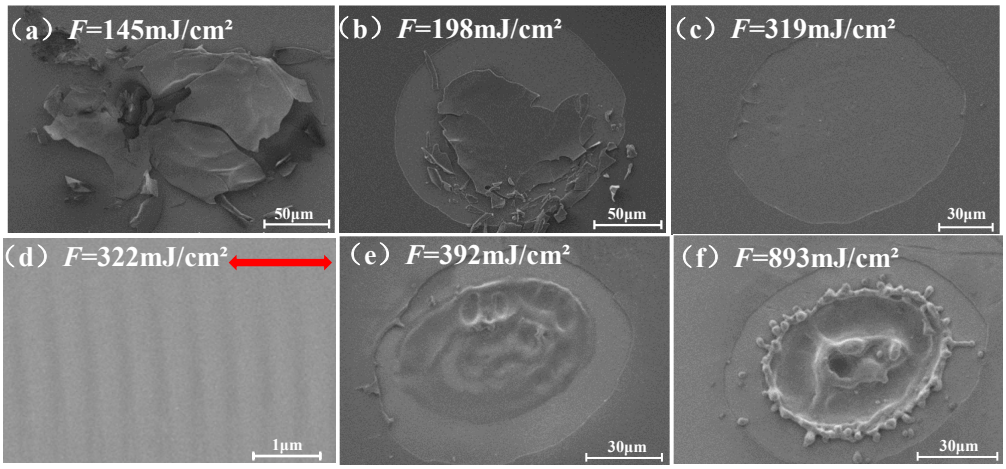

Fig. 3 SEM images of the surface topography of 620 nm photoresist irradiated with different laser fluences. (a) F=145 mJ/cm², (b) F=198 mJ/cm², (c) F=319 mJ/cm², (d) F=322 mJ/cm², (e) F=392 mJ/cm² and (f) F=893 mJ/cm². The red arrow indicates the polarization direction of the laser beam. The number of laser pulses is N=5.

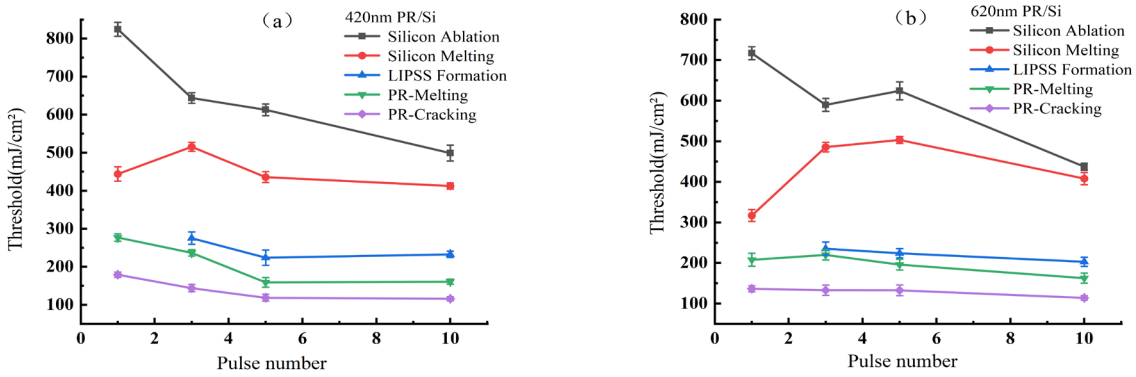

Fig. 4 Changes in morphological thresholds as the number of pulses increases from 1 to 10 under different photoresist thicknesses. (a)420nm photoresist/silicon substrate. (b)620nm photoresist/silicon substrate.

the rapid removal of the surface-bound material. This is consistent with the thermal effects observed by Aslam when laser irradiation is applied to silicon surfaces in ambient air[18]. As the laser fluence decreases below the ablation threshold but remains sufficient to induce melting, the silicon surface undergoes significant morphological changes due to melting and material flow.

Compared to silicon, photoresists have a much lower melting temperature (~423-473 K), allowing them to melt at lower laser fluences. When the laser fluence reaches the melting threshold of the photoresist, the material begins to curl and shrink under irradiation, accompanied by a significant increase in mobility and a decrease in viscosity. At even lower laser fluences, thermal expansion and fragmentation of the photoresist surface occur due to the combined effects of thermal and mechanical stresses during irradiation (**Figure 2(e)** and **Figure 3(a)**). Additionally, OM images reveal the bright surface modifications at low laser fluences, caused by the aggregation and absorption of laser energy. These modifications are attributed to photoresist molecular pyrolysis and chemical structure changes [16], as highlighted in **Figure 2(f)**.

As observed in **Figure 3**, LIPSS still form despite the silicon substrate surface being covered with a photoresist film layer. This phenomenon indicates that the photoresist layer failed to completely eliminate or shield the coupling between the strongly polarized laser and the surface electromagnetic waves scattered and excited by the silicon substrate surface. The interference effects triggered by this coupling constitute the key mechanism for LIPSS formation. Typically, the formation of LIPSS is commonly explained by the interference of the incident laser with surface electromagnetic waves scattered or excited due to surface roughness, leading to periodic energy deposition and surface modification. A critical mechanism in this process involves the excitation of surface electromagnetic waves [19,20], particularly the formation of SPP [21-23].

SPP excitation at a planar interface requires the real part of the dielectric constant of the material on one side of the interface to be negative and smaller than the negative real part of the dielectric constant of the medium on the other side (for a metal-air interface, i.e., $\mathrm{Re}(\varepsilon_m) < -1$) [24]. Although photoresist films and silicon substrates are typically regarded as non-plasmonic materials [25]. However, under pulsed laser irradiation, the silicon surface undergoes significant changes. Specifically, through nonlinear ionization processes, the electron density in the silicon conduction band increases significantly, forming a dense electron-hole plasma. This causes the real part of silicon's dielectric function to become negative at the laser wavelength (532 nm), resulting in transient metallization [17]. This transformation enables the silicon surface to become a plasmonically active material capable of supporting SPP excitation.

This transient 'metallic-like' optical response on silicon surfaces provides a plausible mechanism for explaining LIPSS formation under these conditions. It enables the surface to couple photons and excite SPPs, leading to periodic modulation of the surface. Therefore, this paper argues that the period of LIPSS is primarily determined by the period of SPP, i.e., $\Lambda_{LIPSS} \approx \Lambda_{SPP}$. The value of λ_{SPP} is determined by the dielectric constants of the two media and the wavelength of the incident laser [26]. This research, λ_0=532 nm, ε'_S=−14.2 [27], ε_d=1 [28]. The cycle can be expressed as:

$$\lambda_{SPP} = \lambda_0 \sqrt{\frac{\varepsilon'_s + \varepsilon_d}{\varepsilon'_s \cdot \varepsilon_d}} \quad (1)$$

The resulting theoretical period is ~513 nm. This theoretical value agrees closely with the experimentally observed average LIPSS period (530 ± 5 nm). This indicates that the theoretical model employed can effectively predict and explain the formation of LIPSS in this experiment.

As shown in **Figure 4**, the threshold for LIPSS formation show a decreasing trend with the increase of the number of laser pulses under different film thickness conditions. However, this study observed a phenomenon worthy of further investigation: after a specific number of pulses (e.g., N=3 or N=5), the energy threshold required to induce specific surface morphologies (such as silicon melting) exhibits a slight rebound. For instance, when the photoresist thickness is 420 nm, the silicon melting threshold under N=3 pulses is slightly higher than that under N=1; when N=5, the silicon melting and ablation thresholds under a 620 nm thick film are slightly higher than those under a 420 nm thick film.This may be related to thermal diffusion and stress accumulation, where thermal diffusion expands and causes localized thermal stress release. Although this trend is small, it indicates the complexity of the nonlinear correspondence and dynamic evolution during laser-induced surface topography changes.

Feedback effects play a significant role in multi-pulse laser irradiation. Single-pulse laser exposure results in surface roughness with defects and photoresist melting. These rough surfaces, defects, and photolysis products may contribute to the coupling of energy from subsequent laser pulses and promote laser absorption on the material surface. As this process is repeated, the positive feedback effect triggered by multi-pulse laser exposure favours the formation of ripple structures [29]. This is precisely why LIPSS does not occur when the pulse count is 1.

Experimental evidence shows that the expansion of laser-induced ablation plumes is hindered by the presence of the confinement layer [30]. As the laser interacts with the material, the laser energy is rapidly absorbed by the material surface when the laser energy exceeds a certain fixed threshold. This results in localized areas of melting, vaporization and the formation of high temperature, high density plasma clouds following ionization. The expansion of the plasma can lead to the generation of high-pressure excitations, which induced excitation stress develops with the laser energy [31].

Figure 5 schematically illustrates the generation of plasma under two conditions: without film confinement and with film confinement. **Figure 5(a)** shows the unconfined pure silicon sample surface model, where the laser can act directly on the pure silicon surface. At this condition the plasma is not constrained by the outside surroundings and is free to expand outwards. The energetic particles of the plasma interact with the silicon atoms, leading to the removal and reorganization of the surface atoms, resulting in the formation of ordered microscopic textures. These tex-

tures are usually caused by the interference between the incident laser beam and the scattered waves from the surface [32,33]. This interference results in periodic modulation of energy deposition, thereby forming patterns on the material surface.

When using a confinement layer with photoresist, the high temperature and high-pressure cloud generated by the plasma extends the interaction time with the silicon substrate under the expansion constraint of the photoresist. This allows the silicon substrate to absorb most of the laser energy, thus rapidly warming up and facilitating the formation of LIPSS at a lower laser energy density. After the ablation of the photoresist, LIPSS is observed on the silicon surface, as shown in **Figure 5(c)**. The weak absorption of the photoresist layer at 532 nm ensures that incident energy can effectively penetrate and act upon the silicon substrate, consistent with our observations of melting and phase transitions occurring on the silicon surface.

Side by side, it proves that the penetration ability of laser energy to photoresist layer is relatively stable within a certain thickness range. When the film thickness varies within a certain limit, the plasma is still able to effectively act on the silicon surface, thus maintaining the LIPSS formation threshold.

5. Conclusion

The formation of LIPSS on a silicon substrate through nanosecond pulses (λ=532 nm, τ=8 ns) is experimentally demonstrated with a restraining layer of photoresist.The results show that the formation of LIPSS depends on the laser parameters, including the laser energy density and the number of pulses. The period of LIPSS is in the range of 530 ± 5 nm and the direction of LIPSS is perpendicular to the laser polarization direction.

Experimental results indicate that the coupling process between plasma and laser energy promotes the formation of LIPSS. Under laser irradiation, the photoresist on the surface of the silicon substrate changes the behaviour of the surface plasma, which in turn exerts a modulation effect on the energy distribution and excitation of the plasma. This modulation effect is manifested in the way that the photoresist affects the local intensity distribution and surface wave propagation characteristics of the plasma by absorbing laser energy and changing the local electron density, thus significantly affecting the formation process of LIPSS.

This study contributes to a better understanding of the laser processing mechanism under layered structures and promotes the potential application of laser micromachining technology.

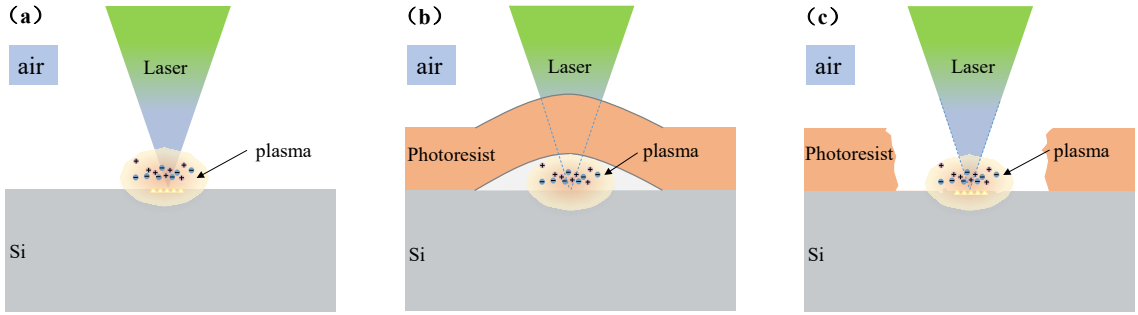

Fig. 5 illustrates the laser-induced plasma generation on the surface of pure silicon samples with and without a photoresist confinement layer. (a) surface Model of Pure Silicon Samples Without Constraint Layers. (b) and (c) represent surface models of pure silicon samples with a constrained layer.

Disclosures

The authors declare no conflicts of interest.

Data availability

The data that support the findings of this study are available from the corresponding author upon reasonable request.

Acknowledgements

This work has been sponsored by “Shanghai Sailing Program (No.21YF1416200)”, National Natural Science Foundation of China (No.12104288) and funded by the Experimental team construction project.

References

[1] A. Ali, P. Piatkowski, and A. S. Alnaser: Materials., 16(6), (2023) 2184.
[2] D. Gallego, I. Ayerdi, A. Pan, S. M. Olaizola, and A. Rodriguez: Sci. Rep., 15(1), (2025) 15483.
[3] J. Outon, M. Carbu, M. Dominguez, J. J. Delgado, V. Matres, and E. Blanco: Surf. Interfaces., 57, (2025) 105780.
[4] J. Song, H. Wang, X. Huang, L. Huang, Y. Jiang, W. Yin, Q. Yao, and Y. Dai: J. Opt. Soc. Am. B., 40(6), (2023) 1413.
[5] S. Yang, Q. Xian, Y. Liu, Z. Zhang, Q. Song, Y. Gao, and W. Wen: J. Funct. Biomater., 14(4), (2023) 208.
[6] Z. Zhou, X. Ou, Y. Fang, E. Alkhazraji, R. Xu, Y. Wan, and J.E. Bowers: eLight., 3(1), (2023) 1.
[7] J. Bonse, S. Höhm, S.V. Kirner, A. Rosenfeld, and J. Kruger: IEEE J. Sel. Top. Quantum Electron., 23(3), (2017) 9000615.
[8] R.D. Murphy, B. Torralva, D. P. Adams, and S. M. Yalisove: Appl. Phys. Lett., 104(23), (2014) 1.
[9] Y. Ren, S. Luo, P. An, L. Zhao, Y. Cai, and Z. Li: Appl. Phys. Lett., 125(3) (2024) 031109.
[10] A. G. Kovacevic, S. Petrovic, B. Bokic, B. Gakovic, M. T. Bokorov, B. Vasic, R. Gajic, M. Trtica, and B. M. Jelenkovic: Appl. Surf. Sci., 326, (2015) 91.
[11] W. L. Barnes, A. Dereux, and T. W. J. n. Ebbesen: Nature.,424(6950), (2003) 824.

[12] D. Kochuev, R. Chkalov, and A. Chernikov: Materials Today: Proceedings., 19(043), (2019) 1928.
[13] H. Matsuta and K. Wagatsuma: Appl. Spectrosc., 56(9), (2002) 1165.
[14] B. N. Chichkov, M. Carsten, N. Stefan, V. A. Ferdinand, and T. Andreas: Appl. Phys. A., 63(2), (1996) 109.
[15] K. Zimmer, M. Ehrhardt, P. Lorenz, X. Wang, C. Vass, T. Csizmadia, and B. Hopp: Appl. Surf. Sci., 302, (2014) 42.
[16] S. Lai, Y. Liu, Y. Zhao, C. Zhang, and B. Han: Opt. Laser Technol., 168, (2024) 109871.
[17] M. Ehrhardt, B. Han, F. Frost, P. Lorenz, and K. Zimmer: Appl. Surf. Sci., 470, (2019) 56.
[18] N. Aslam, T. M. Khan, M. Q. Javed , A. Rehman, S. A. Abbasi, A.Shah, and M. Raffi: Surf. Interfaces., 41, (2023) 103252.
[19] P. Temple and M. Soileau: IEEE J. Quantum Electron., 17(10), (1981) 2067.
[20] A. M. Bonch-Bruevich, M. N. Libenson, V. S. Makin, and V. V. Trubaev: Opt. Eng., 31(4), (1992) 718.
[21] F. Keilmann and Y. Bai: Appl. Phys. A., 29, (1982) 9.
[22] J. Bonse, J. Krüger, S. Höhm, and A. Rosenfeld: J. Laser Appl., 24(4), (2012) 042006.
[23] P. Lorenz , A. Lotnyk , M. Ehrhardt, and K. Zimmer: J. Laser Micro Nanoeng., 20(3), (2025)212.
[24] H. Raether: Springer Tracts Mod. Phys., 111, (1988) 136.
[25] Atwater, Harry A: Sci. Am., 296(4), (2007) 56.
[26] F. Garrelie, J.P. Colombier, F. Pigeon, S. Tonchev, N. Faure, M. Bounhalli, S. Reynaud, and O. Parriaux: Opt. Express., 19(10), (2011) 9035.
[27] Jr G. Jellison and D. Lowndes: Appl. Phys. Lett., 51(5), (1987) 352.
[28] M. R. Querry: Chemical Research, Development & Engineering Center.US Army Armament Munitions Chemical Command,(1998) 29.
[29] J. Bonse, A. Rosenfeld, and J. Krüger: J. Appl. Phys., 106(10), (2009) 1.
[30] T.J.Y. Derrien, J. Krueger, and J. Bonse: J. Opt., 18(11), (2016) 1.
[31] E. G. Gamaly, S. Juodkazis, K. Nishimura, H. Misawa, B. Luther-Davies, L. Hallo, P. Nicolai, and V. T. Tikhonchuk: Phys. Rev. B: Condens. Matter Mater. Phys., 73(21), (2006) 214101.
[32] J. E. Sipe, J. F. Young, J. S. Preston, and H. M. van Driel: Phys. Rev. B., 27(2), (1983) 1141.
[33] M. Wang and S. Lai: CIOT 2025., 13994, (2025)191.

(Received: December 1, 2025, Accepted: January 31, 2026)